UNIVERSITY OF BATH

Citation for published version:
Rastetter, B, Wright, S, Gheduzzi, S, Miles, A & Clift, S 2016, 'The influence of tibial component malalignment on bone strain in revision total knee replacement.', *Proceedings of the Institution of Mechanical Engineers, Part H - Journal of Engineering in Medicine*, vol. 230, no. 6, pp. 561. https://doi.org/10.1177/0954411916638684

DOI:
10.1177/0954411916638684

Publication date:
2016

Document Version
Peer reviewed version

Link to publication

University of Bath

Alternative formats
If you require this document in an alternative format, please contact:
openaccess@bath.ac.uk

General rights
Copyright and moral rights for the publications made accessible in the public portal are retained by the authors and/or other copyright owners and it is a condition of accessing publications that users recognise and abide by the legal requirements associated with these rights.

Take down policy
If you believe that this document breaches copyright please contact us providing details, and we will remove access to the work immediately and investigate your claim.

Download date: 05. May. 2023

Original Article

Corresponding author:

Benjamin R. Rastetter, Centre for Orthopaedic Biomechanics, Department of Mechanical Engineering, University of Bath, Bath, BA2 7AY, United Kingdom

Email: B.Rastetter@bath.ac.uk

The influence of tibial component malalignment on bone strain in revision total knee replacement.

Benjamin R Rastetter, Samantha J Wright, Sabina Gheduzzi, Anthony W Miles, Sally E Clift

Centre for Orthopaedic Biomechanics, Department of Mechanical Engineering, University of Bath, Bath, UK

Abstract

Revision total knee replacement is a challenging surgical procedure typically associated with significant loss of bone stock in the proximal tibia. To increase the fixation stability, extended stems are frequently used for the tibial component in revision surgery. The design of the tibial stem influences the load transfer from tibial component to the surrounding bone and is cited as a possible cause for the clinically reported pain in the location of the stem-end. This study aimed to analyse the strain distribution of a fully cemented revision tibial component with a validated finite element model. The model was developed from a scanned composite tibia (Sawbones), with an implanted, fully cemented stemmed tibial component aligned

to the mechanical axis of the tibia. Loading was applied to the tibial component with mediolateral compartment load distributions of 60:40 and 80:20. Three strain gauged composite tibias with implanted tibial components of the same design using the same loading distribution were tested to obtain experimental strains at five locations in the proximal tibia. The finite element model developed was validated against strain measurements obtained in the experimental study. The strains displayed similar patterns (R^2=0.988) and magnitudes with those predicted from the finite element model. The displacement of the stem-end from the natural mechanical axis in the finite element model demonstrated increased strains in the stem-end region with a close proximity of the distal stem with the cortical bone.

The simulation of a mediolateral compartment load of 80:20 developed peak cortical strain values on the posterior-medial side beneath the stem. This may possibly be related to the clinically reported pain at the stem-end. Furthermore, stem positioning in close proximity or contact with the posterior cortical bone is a contributory factor for an increase in distal strain.

Keywords

Revision total knee replacement, arthroplasty, finite element, experimental validation, cemented implant

Introduction

Total knee replacement (TKR) is a common and generally successful procedure with over 80,000 surgeries being carried out each year in the United Kingdom.[1] Statistics from national joint registries or clinical studies show that increasing numbers of young and more active patients are currently being considered for surgery, and this is potentially leading to a rise in revision TKR.[1,2] A challenging aspect in revision TKR is the significant bone loss associated with bone resections

from primary TKR, implant removal, fracture, infection, stress shielding and osteolysis.[3,4] To increase the stability and improve fixation of the tibial component, extended stems are commonly used in revision surgery. A frequently reported complication is pain in the area of the stem-end attributed to the increased load transfer and stress concentration in the surrounding bone. Clinical studies show that pain at the stem-end in the tibia is mainly associated with the hybrid fixation technique with a cemented tibial tray and a press-fit stem.[5-7] However, a small number of cases of pain have also been reported with fully cemented implants.[6] To reduce the risk of pain, slotted press-fit stems have been used to reduce stress concentration at the stem end.[6,8] In addition, a concept stem with a polyethylene tip has demonstrated an improved stress distribution by reducing the stiffness of the material at the stem tip.[9] Completo et al.,[10] in an experimental study of the polyethylene tip, linked a malaligned knee with an abnormal condylar load distribution as a possible contributory factor to stem-end pain.

To predict the biomechanical behaviour of new implant designs that are challenging to measure experimentally, the computational finite element method is commonly used. To validate these computational models, it is essential to compare the results with experimental data to demonstrate that the FE model provides a realistic representation.[11] The variability of cadaveric bone is problematic for the reliability and repeatability in *in vitro* experimental studies of load transfer in the tibia in TKR. Therefore, standardised synthetic composite bone models are commonly used with structural properties that have been proven to represent the mechanical properties of cadaveric bone.[12]

The aim of this study was to develop a validated FE Model for a fully cemented tibial component to facilitate the evaluation of strain concentrations at the stem-end.

Materials and Methods

Experiments

Three experimental test specimens using fourth-generation composite tibias (medium left, 3401, Sawbones®, Vashon, WA, USA) were used in the study. These were implanted according to surgical procedure with a fully cemented tibial component of the Triathlon TS Knee System

(Stryker, Kalamazoo, MI, USA) with a Co-Cr universal baseplate (size 4). Due to only one Triathlon Co-Cr stem being available, additional stems manufactured in stainless steel with the same geometry were used in the study (100 mm stem length and 12 mm diameter) (see Figure 1).

[Insert Figure 1.]

Figure 1: Manufactured cemented stem (a) used experimentally and original Triathlon TS stem (b).

A standardised procedure was used to resect the tibial plateau at 11 mm measured from the highest point of the tibial plateau. The distal ends of the composite tibias were removed by cutting at a location 210 mm from the proximal resection plane and fixed in aluminium pots with a low melting point alloy (MCP70; Mining & Chemical Products, Wellingborough, UK) to allow for mounting the test specimens in the testing machine. Three-element 'rectangular' strain gauge rosettes (1-RY91-6/350, HBM, Darmstadt, Germany) were positioned based on a previous digital image correlation study to asses areas of interest and past published research.[13] The strain gauges were placed at three posterior locations; 38 , 88 and 143 mm from the most proximal point of the tibia and one on the medial and the other on the lateral surface of the tibia at 45 mm from the proximal point (see Figure 2). A load of 500 N was applied through the femoral component and polyethylene insert using a hydraulic test machine (HBT 25-200; Zwick Roell, Ulm, Germany) with a 60:40 mediolateral compartment load distribution typical to that of a normal knee.[14] The specimens were positioned on the rig using a series of location and alignment jigs. In addition, the test rig allowed adjustment in the coronal plane to set the mediolateral ratio and a degree of freedom axially in the traverse plane. The applied load of 500 N is less than the typical physiological loads experienced in the knee (see Figure 3). It was selected because of limitations in the Tekscan Flexiforce sensors (A201; Tekscan, Inc., South Boston, MA, USA) used in the experimental study to regulate the compartmental load share.[13] Since the aim of this study was to validate the finite element analysis (FEA) model, as long as the loading conditions were replicated in the two approaches, the fact that this load was less than normal physiological loads was considered acceptable.

[Insert Figure 2.]

Figure 2: Comparison of strain gauge locations: (a) reference central notch intact tibia, (b) experimental sample, (c) posterior view with global axis system, (d-e) lateral-medial view with localized 1 mm surface mesh.

[Insert Figure 3.]

Figure 3: Set up of experimental strain gauge study.

Finite element analysis

The bone geometry for the FEA was developed from (CT) scans of a fourth-generation composite tibia. The surface model contained two material layers: cortical bone and cancellous bone with an intramedullary canal. Computer-aided design (CAD) software, Catia V5 (Dassault Systemes, Velizy, France) was used to separate the surface layers and patch the distal connection point. Boolean operations created a multi-body part to replicate the geometry of the composite tibia. A Triathlon TS tibial component was measured with a Vernier calliper and the basic geometry reconstructed as a CAD model. A 1 mm thick cement mantle was used to model the fixation of the tibial component (tray and stem) and the intramedullary canal below the stem tip was filled with cement replicating the experimental specimens. To develop the required tibial component position, the stem was aligned to the mechanical axis of the tibia taking account of the reported range of 7° posterior slope.[15,16]

The initial analysis was performed with the knee system built in 3° posterior slope positioning the stem centred in the cancellous bone and perpendicular to the canal axis in the coronal plane (see Figure 4). In addition, the posterior slope was modified in 1° steps (from 1° to 6°) and two models created with a medial/lateral stem offset of 1.8 mm to the canal axis simulating multiple stem-end positions.

[Insert Figure 4.]

Figure 4: Tibial component installation and alignment of stem-end to the intramedullary canal axis.

Young's modulus for cortical and cancellous synthetic material, 16.7 GPa and 0.155 GPa, respectively, were obtained from manufacturers' material data sheets.[17] The Young's Modulus for cement and the Co-Cr implant, 2.28 GPa and 210 GPa, respectively, were selected from previous FEA studies on revision TKR.[9,18] All materials were assumed to have a Poission's ratio of 0.3, to be isotropic and with linear elastic behaviour. The FEA software Ansys Workbench 15.0 (Ansys, PA, USA) was used for the analysis and to generate the mesh for all components, formed out of 10-node quadratic tetrahedral elements adequate for complex bone geometries.[19] The element sizes were based on the maximum feasible for the curvature and sharp angles of the model geometry in the classical environment (Ansys Parametric Design Language (APDL)) with 3 mm elements for the cortical body, 2 mm for the cancellous and implant body, 1 mm for the cement mantle and a surface mesh of 1 mm at the strain gauge locations, leading to 295,006 elements and 478,220 nodes distributed over the complete FE model (see Figure 5).

[Insert Figure 5.]

Figure 5: Anterior-posterior sectional view showing the mesh applied to the four bodies.

For the boundary conditions, a bonded contact was assumed for all surface connections and a fixed support was created at the distal cut. A load of 500 N was applied directly to the tibial tray with a 15 mm diameter contact patch in a central location of each compartment. Two scenarios were compared simulating a distribution of 60:40 and 80:20 mediolateral.[8,9,14] The three-element strain gauge rosettes used for the experimental analysis were idealised as 6x6 mm square and projected with a depth of 0.001 mm on the cortex of the tibia. A local axis system was created at each gauge surface to measure the normal strain in the y-axis as illustrated in Figure 6.

[Insert Figure 6.]

Figure 6: Measurement area (6x6 mm) with local axis system at strain gauge location P143 (Figure 2) in the stem-end region.

Results

Model validation

In the experimental study, a load of 500 N with a mediolateral compartmental load distribution of 60:40 was applied to three bone samples. The normal strains in the vertical direction (y-axis) at each gauge location were measured with three repeats. The mean value at each location was determined along with the standard deviations. The FEA results were measured over a 6x6 mm area and the mean value was determined for the five locations (see Table 1). The strains in both analyses demonstrate a similar pattern with an increase from proximal to distal region of the tibia. The regression line of the five vertical strain values had a slope of 1.34, a coefficient of determination of 0.988 and a root mean square error (RMSE%) of 2.5% (see Figure 7). The simulation of a malaligned knee with a load distribution of 80:20 displays a shift of proximal strain medially with tensile strain measured at the lateral strain gauge and an small compressive strain increase of -11 με (5%) at the distal locations P143 compared to the FEA results with a 60:40 load distribution.

[Insert Figure 7.]

Figure 7: Linear regression between predicted FEA and experimental strains.

		Force	Microstrain				
			L45	P38	M45	P88	P143
Exper. results (3 repeats)	Mean value	500 N 60:40 M:L	-43	-71	-37	-110	-279
	SD		4	5	7	2	15
FEA results	Mean value	500 N 60:40 M:L	-24	-44	-34	-90	-204
		500 N 80:20 M:L	17	-31	-73	-88	-215

Table 1: Comparison of experimental and FEA normal strain results measured from the vertical grid and the local y-axis with the 3° posterior sloped model.

Contour plots of the normal strain to the global y-axis (see Figure 2) of both load scenarios illustrate the effect of proximal strain shielding from the Co-Cr implant and the load transfer to the region of the stem-end (see Figure 8). The peak compressive strain in the cortical bone develops around 30 mm beneath the stem-end with a posterior-medial orientation. In addition, with an 80:20 load distribution (Figure 8b) the peak cortical strain increases by 67% from -300 με (a) to -500 με (b) with a further overall shift to the posterior-medial side.

[Insert Figure 8.]

Figure 8: Posterior view of the normal strain to the global y-axis (Figure 2) with a medial-lateral load distribution of (a) 60:40 (b) 80:20

Stem-end positions

The analysis with a mediolateral load distribution of 60:40 of different stem-end positions with the modification of the posterior slope angle creates three types of implant-cement to bone interfaces: 1° slope with posterior contact of cement to cortical bone, 2° and 3° slope with no contact to cortical bone and 4° to 6° slope with anterior-medial contact to cortical bone. The strains were measured at the identical cortex locations with a posterior angle from 1° to 6° and medial and lateral offset of 1.8 mm as illustrated in Table 2. At the location P143, the strains increase with a closer posterior stem location and have its largest increase of 45 με with contact of cement to cortical bone. The proximal strains (L45, P38, M45 and P88) are the highest with a posterior slope of 2° and 3° where the implant is fully surrounded by a cancellous bone layer and demonstrates an abrupt decrease with cement-cortical bone contact. This is again shown with the medial (with contact) and lateral offset stem. The normal strain distribution for the four main simulated stem positons are illustrated in Figure 9. A strain concentration develops beneath the stem tip with values up to -1100 με (see Figure 10). The peak compressive strain on the cortex develops with a posterior implant-cement contact to the cortical bone with a magnitude of -340 με. The centred stem with a 3° posterior slope (Figure 9f) has a cortex strain of -300 με. A further reduction to -280 με (Figure 9g) was observed

with the stem in close proximity to the anterior cortical bone. Furthermore, the medial and lateral 1.8 mm offset positioned stem did not show any major change in strain distribution.

Posterior slope	Min. distance (x) cement to cortical (mm)	Offset (x) stem end to shaft axis (mm)	Mean microstrain (local y-axis)				
			L45	P38	M45	P88	P143
1°	-0.6	3.2	-13	-29	-25	-61	-282
2°	1.4	1.9	-25	-42	-33	-92	-237
3°	3.2	-2.5	-24	-44	-34	-90	-204
4°	1.3 (am -0.5)	-4.3	-18	-35	-30	-74	-173
5°	-0.6	-6.3	-15	-31	-28	-66	-144
6°	-2.6	-8.4	-13	-29	-27	-60	-114
3°	0.2 (lateral)	1.8 (lateral)	-18	-42	-35	-89	-202
3°	-0.5 (medial)	1.8 (medial)	-21	-33	-23	-72	-203

Table 2: Predicted strain results and stem-end positions for the modified angular resection surface and parallel medial/lateral offset.

[Insert Figure 9.]

Figure 9: Normal strain distribution (global y-axis) at the stem-end area: sagittal cut, posterior view, (a,e) 1° posterior slope, (b,f) 3° posterior slope, (c,g) 6° posterior slope; frontal cut, posterior view, (d,h) medial 1.8 mm offset stem.

Discussion

The aim of this study was to develop a FE model of a synthetic tibia implanted with a tibial component used in revision TKR and the evaluation of the load transfer to the area of the stem-end. The comparison of experimental and computational strain results demonstrated a good correlation that validates the FE model. Although the overall lower FEA values with a regression slope of 1.34 is higher than in previous studies,[11,18,20] it is likely to be a result of developing a model representing an ideal implantation condition with fully bonded body contact pairs and an ideal material structure. The slightly lower elastic modulus of the manufactured stems used

experimentally and the value of 210 GPa used in the FE model had a limited effect on the overall magnitude of strain. Furthermore, the simplified stem geometry in the FE model with exclusion of the fluted surface has no implication with a fully bonded simulation.

The simulation of a malaligned knee with a load distribution of 80:20 demonstrates that an increased bending moment applied to the implanted tibial component produces a concentration of strain in the distal stem region in the tibia. This finding supports the thesis that pain at the stem-end may be associated with a malaligned knee.[10] Skeletal pain has been cited to originate on the sensitive periosteum, a layer on the cortex of the tibia, and nerve stimulation associated with dimensional deviations.[10,21,22] Therefore, this study was focused on the strain development on the outer surface of the cortical bone. The 67% increase of strain in the stem-end area demonstrates the importance of recreating the natural knee alignment in TKR. Although pain at the stem-end is mainly reported with long cementless stems, some complications with fully cemented stems have been documented in clinical studies.[6,7] This is possibly a result of a more challenging surgical procedure to achieve a well-aligned knee with the use of press-fit stems.[23]

[Insert Figure 10.]

Figure 10: Detailed views of regions with peak strain (Figure 9): local strain concentration beneath the stem tip (a) and maximal cortex strain (b).

The investigation on the influence of stem-end orientation with respect to the natural mechanical axis of the bone demonstrated that the highest reduction of strain in the stem-end region occurred with an implantation anterior to the natural axis with a 4° to 5° posterior slope of the resection surface. However, a further anterior stem orientation (see Figure 9g) increases torsion with a shift of tensile strains to the posterior cortical bone. The ideal positioning of the stem-end in this case is in a range from natural bone axis (2° slope) towards an anterior position without cortical contact (3° slope) to develop a small increase in proximal strain and therefore reduce stress shielding. This effect of this extent may not be possible with the current 12 mm diameter fully cemented stem in the FEA considering the relatively thin cement thickness without cement penetration into the

cancellous bone. A contributing factor to reduce the risk of stem-end pain by avoiding close implantation of the stem-end to the posterior cortical bone increasing the strain acting on the thinnest cortical layer. The malalignment of the stem-end in the intramedullary canal in the millimetre range proved to have an influence on the load transfer to the distal tibial bone. The implant installation without precise analysis of the experimental samples is a limitation for the validation of the FE model, although it may support the use of computer-assisted surgery tools to produce stem alignment close to the intramedullary canal and implant design selection for the variance of bone geometry.[24, 25]

This study had further limitations: for instance, simplified measurements and CAD reconstruction of the implant and cement geometry. Furthermore, a frictional contact was not introduced simulating micromotion between implant and cement a feature that demonstrated improved results mainly with a press-fit stem in Completo et al.'s[20] FEA study. Finally, the simulation of only one loading contact position and the exclusion of the supporting soft tissue represents an over simplification in the analysis of the major forces acting on the knee.

Conclusion

In this study, the development and validation of a FE model of a revision TKR has been presented. The redistribution of the load to the medial side of the tibial plateau associated with a malaligned knee or with abnormal compartment loading created peak strain values beneath the stem-end. In addition, the analysis demonstrated a reduction of strain if the stem-end of the implant was aligned with the natural mechanical axis of the tibia and a small increase of proximal strains reducing stress shielding. Furthermore, the simulation of multiple stem-end orientations revealed that posterior contact or close proximity of the distal stem to the cortical bone may be a contributory factors of the clinically reported stem-end pain

Declaration of conflicting interests

The author(s) declared no potential conflicts of interest with respect to the research, authorship and/or publication of this article.

Funding

The author(s) disclosed receipt of the following financial support for the research, authorship, and/or publication of this article: Enid Linder Charitable Foundation provided the funding for the PhD studentship of one of the authors SJW.

List of references

1. National Joint Registry of England, Wales and Northern Ireland. 10th Annual report 2013, http://www.njrcentre.org.uk/njrcentre/Portals/0/Documents/England/Reports/10th_annual_report/NJR%2010th%20Annual%20Report%202013%20B.pdf (accessed 12 May 2014).
2. Carr AJ, Robertsson O, Graves S, Price AJ, Arden NK, Judge A, Beard DJ. Knee replacement. *Lancet* 2012; 379(9823): 1331-1340.
3. Daines BK, Dennis DA. Management of bone defects in revision total knee arthroplasty. *J Bone Joint Surg Am* 2012; 94(12): 1131-1139.
4. Huten D. Femorotibial bone loss during revision total knee arthroplasty. *Orthop Traumatol Surg Res* 2013; 99(1): S22-33.
5. Barrack RL, Rorabeck C, Burt M, Sawhney J. Pain at the end of the stem after revision total knee arthroplasty. *Clin Orthop Relat Res* 1999; 367: 216-225.
6. Barrack RL, Stanley T, Burt M, Hopkins S. The effect of stem design on end-of-stem pain in revision total knee arthroplasty. *J Arthroplasty* 2004; 19(7): 119-124.
7. Peters CL, Erickson J, Kloepper RG, Mohr RA. Revision total knee arthroplasty with modular components inserted with metaphyseal cement and stems without cement. *J Arthroplasty* 2005; 20(3): 302–308.
8. Kim YH, Kwon OS, Kim K. Analysis of biomechanical effect of stem-end design in revision TKA using digital Korean model. *Clin Biomech* 2008; 23(7): 853-858.
9. Completo, A, Talaia P, Fonseca F, Simões JA. Relationship of design features of stemmed tibial knee prosthesis with stress shielding and end-of-stem pain. *Mater Design* 2009; 30(4): 1391-1397.
10. Completo A, Fonseca F, Simões JA, Ramos A, Relvas C. A new press-fit stem concept to reduce the risk of end-of-stem pain at revision TKA: A pre-clinical study. *Knee* 2012; 19(5): 537-542.
11. Gray HA, Taddei F, Zavatsky AB, Cristofolini L, Gill HS. Experimental validation of a finite element model of a human cadaveric tibia. *J Biomech Eng* 2008; 130(3): 031016.
12. Heiner AD. Structural properties of fourth-generation composite femurs and tibias. *J Biomech* 2008; 41(15): 3282-3284.
13. Wright SJ. *Strain distribution in the tibia as a function of applied loading through a revision total knee replacement.* PhD Thesis, University of Bath, UK, 2015.

14. Halloran JP, Petrella AJ, Rullkoetter PJ. Explicit finite element modeling of total knee replacement mechanics. *J Biomech* 2005; 38(2): 323-333.

15. Bellemans J, Ries MD, Victor J. *Total knee arthroplasty - A guide to get better performance.* Berlin, Heidelberg: Springer-Verlag, 2005, p.27.

16. Hashemi J, Chandrashekar N, Gill B, Beynnon BD, Slauterbeck JR, Schutt RC, Mansouri H, Dabezies E. The geometry of the tibial plateau and its influence on the biomechanics of the tibiofemoral joint. *J Bone Joint Surg Am* 2008; 90(12): 2724–2734.

17. Sawbones, Pacific Research Laboratories, Inc. Biomechanical test materials, http://www.sawbones.com/UserFiles/Docs/biomechanical_catalog.pdf (accessed 23 August. 2014).

18. Cawley DT, Kelly N, Simpkin A, Shannon FJ, McGarry JP. Full and surface tibial cementation in total knee arthroplasty: a biomechanical investigation of stress distribution and remodeling in the tibia. *Clin Biomech* 2012; 27(4): 390-397.

19. Polgar K, Viceconti M, O'Connor JJ. A comparison between automatically generated linear and parabolic tetrahedra when used to mesh a human femur. *Proc IMechE, Part H: J Engineering in Medicine* 2001; 215(1): 85-94.

20. Completo A, Fonseca F, Simões JA. Finite element and experimental cortex strains of the intact and implanted tibia. *J Biomech Eng* 2007; 129(5): 791-797.

21. Mach DB, Rogers SD, Sabino MC, Luger NM, Schwei MJ, Pomonis JD, Keyser CP, Clohisy DR, Adams DJ, O'Leary P, Mantyh PW. Origins of skeletal pain: sensory and sympathetic innervation of the mouse femur. *Neuroscience* 2002; 113(1): 155–166.

22. Mørch CD, Hennings K, Andersen OK. Estimating nerve excitation thresholds to cutaneous electrical stimulation by finite element modeling combined with a stochastic branching nerve fiber model. *Med Biol Eng Comput* 2011; 49(4): 385–395.

23. Bono JV, Scott RD. *Revision total knee replacement*. New York: Springer-Verlag, 2005, p.143.

24. Bäthis H, Perlick L, Tingart M, Lüring C, Zurakowski D, Grifka J. Alignment in total knee arthroplasty - a comparison of computer-assisted surgery with the conventional technique. *J Bone Joint Surg Br* 2004; 86(5): 682-687.

25. Jeffcote B, Shakespeare D. Varus/valgus alignment of the tibial component in total knee arthroplasty. *Knee* 2003; 10(3): 243–247.

Figure 1: Comparison of manufactured cemented stem (a) and original Triathlon TS stem (b).

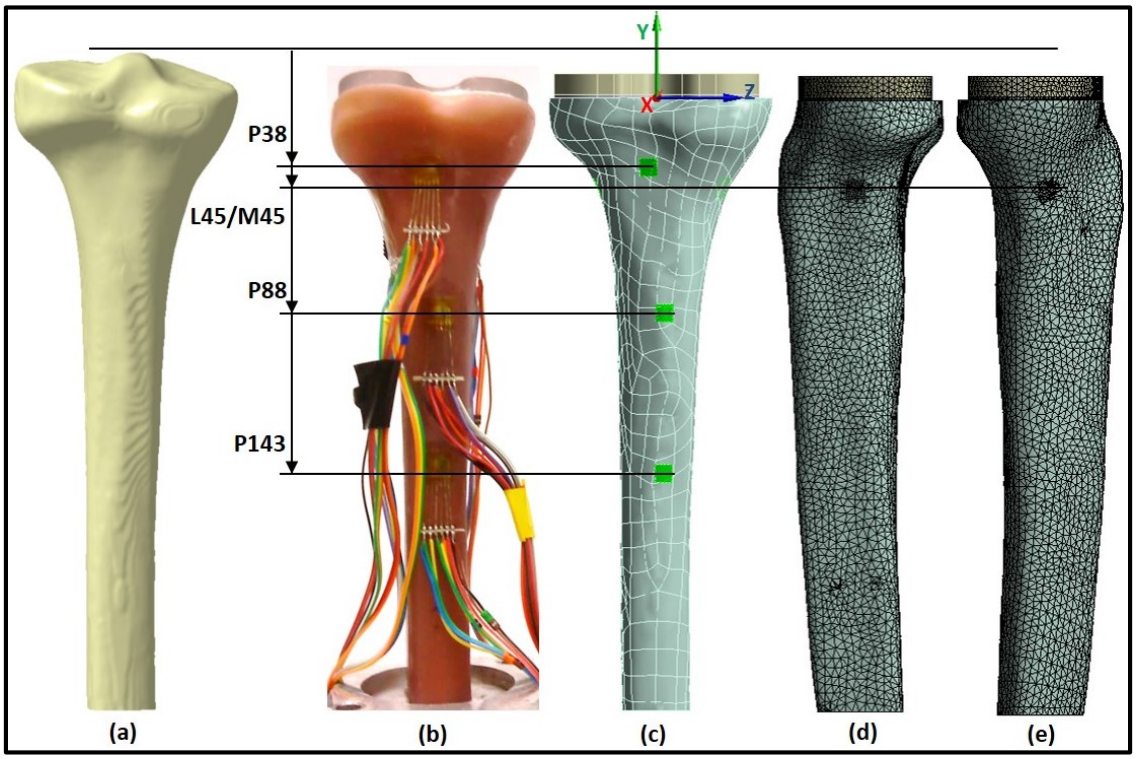

Figure 2: Comparison of strain gauge locations: (a) reference central notch intact tibia, (b) experimental sample, (c) posterior view with global axis system, (d-e) lateral-medial view with localized 1 mm surface mesh.

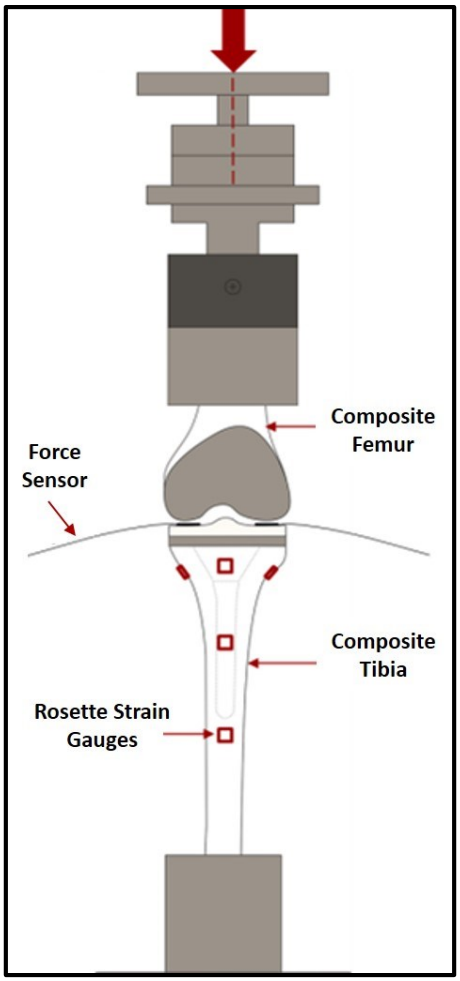

Figure 3: Set up of experimental strain gauge study.

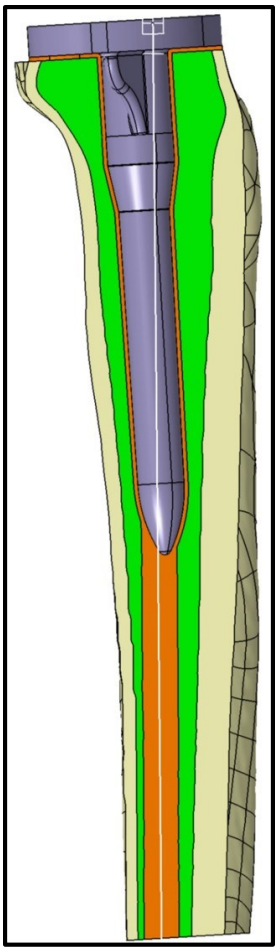

Figure 4: Tibial component installation and alignment of stem-end to the intramedullary canal axis.

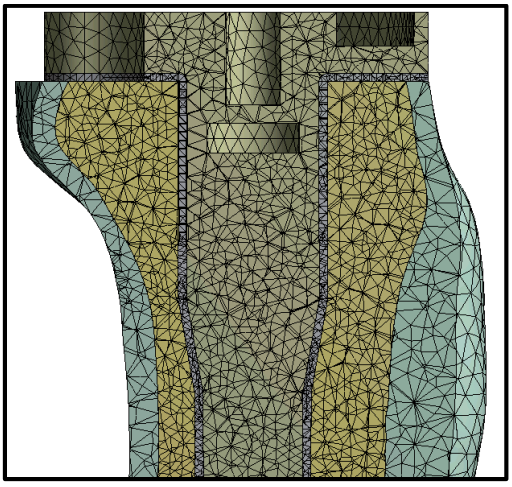

Figure 5: Anterior-posterior sectional view showing the mesh applied to the four bodies.

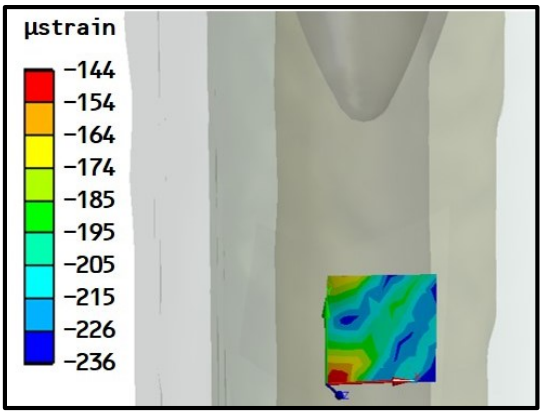

Figure 6: Measurement area (6x6 mm) with local axis system at strain gauge location P143 (Figure 2) in the stem-end region.

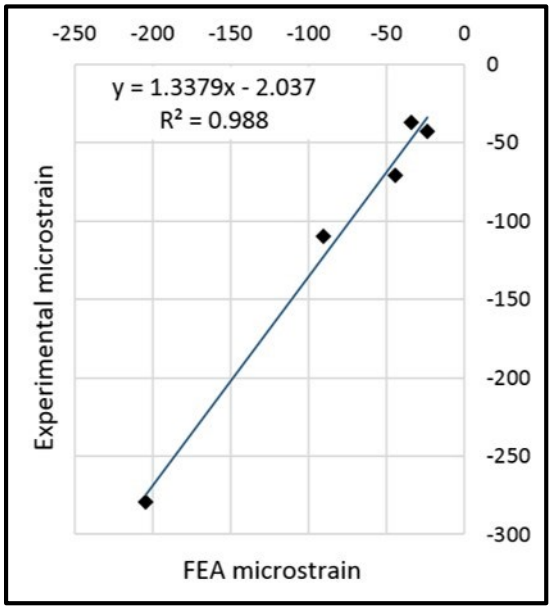

Figure 7: Linear regression between predicted FEA and experimental strains.

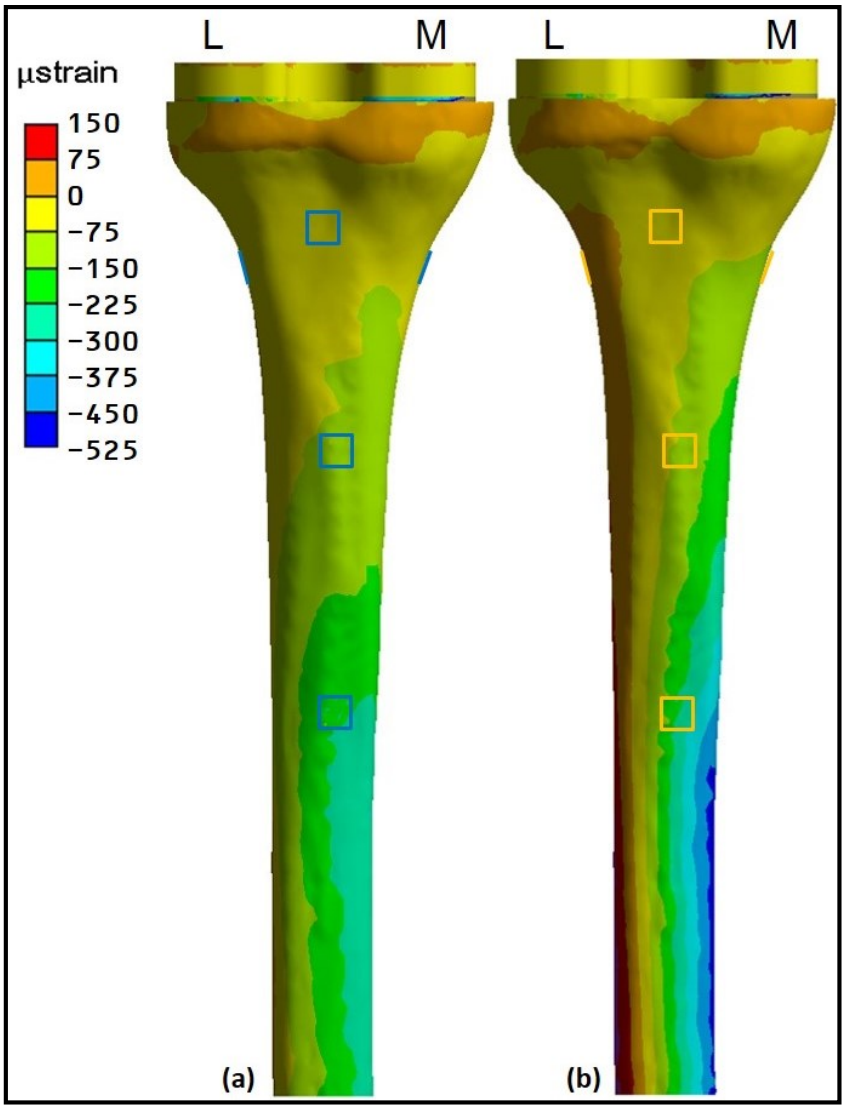

Figure 8: Posterior view of the normal strain to the global y-axis (Figure 2) with a medial-lateral load distribution of (a) 60:40 (b) 80:20

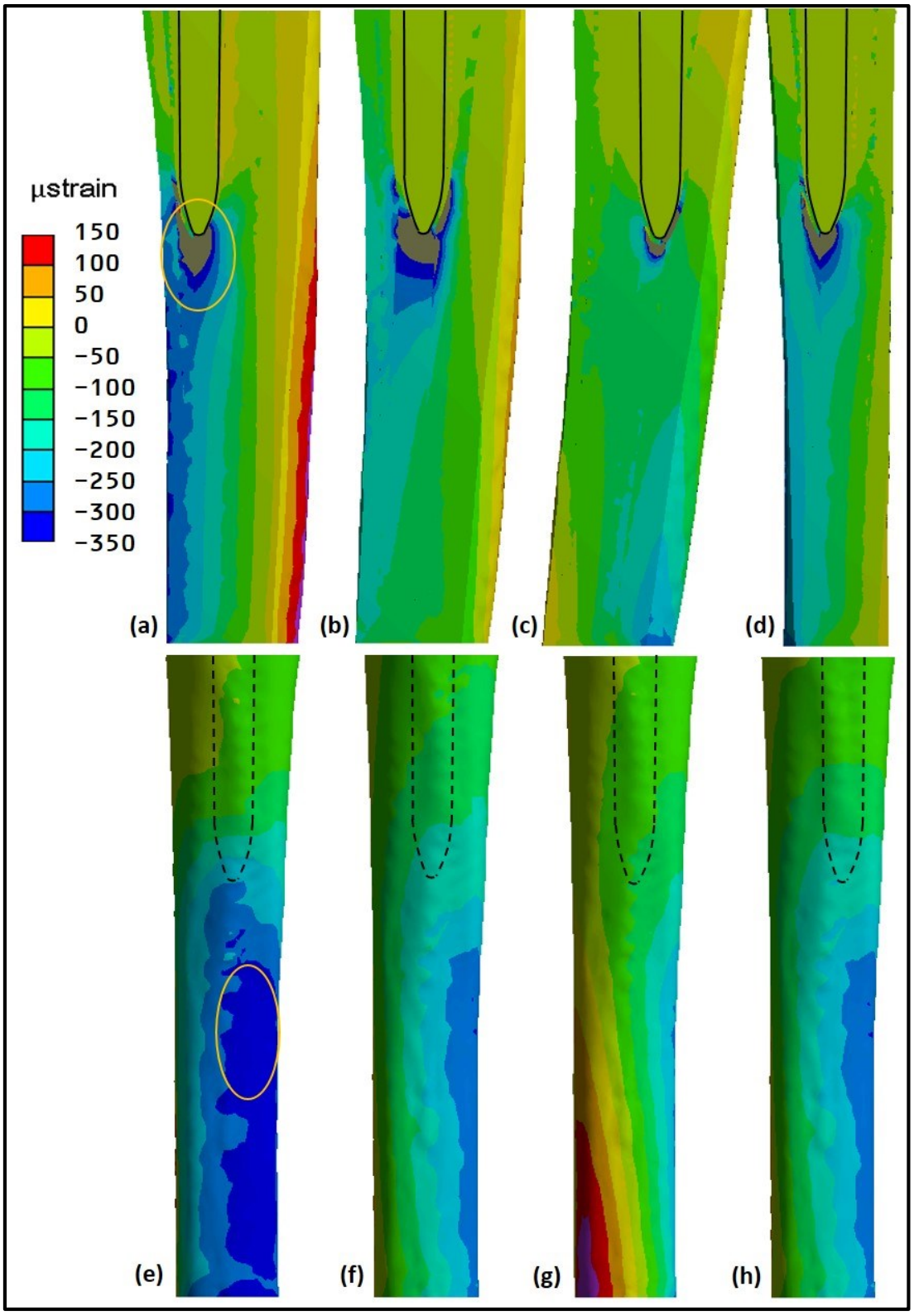

Figure 9: Normal strain distribution (global y-axis) at the stem-end area: sagittal cut, posterior view, (a,e) 1° posterior slope, (b,f) 3° posterior slope, (c,g) 6° posterior slope; frontal cut, posterior view, (d,h) medial 1.8 mm offset stem.

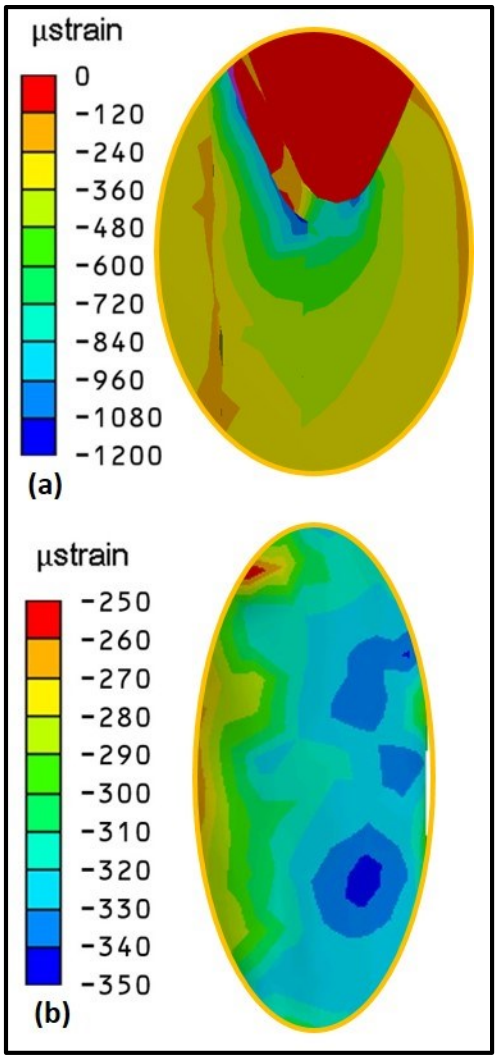

Figure 10: Detailed views of regions with peak strain (Figure 9): local strain concentration beneath the stem tip (a) and maximal cortex strain (b).